BBA - Biomembranes 1868 (2026) 184488

Contents lists available at ScienceDirect

BBA - Biomembranes

journal homepage: www.elsevier.com/locate/bbamem

Research paper

TRAP mediated conformational changes of the human Sec61 channel

Nidhi Sorout, Volkhard Helms *

Center for Bioinformatics, Saarland University, Saarland Informatics Campus, Saarbrücken, Saarland, Germany

ARTICLE INFO

Keywords:
TRAP complex
Sec61 complex
Molecular dynamics simulation
Signal peptide
Protein translocation
Conformational dynamics

ABSTRACT

The integral membrane pore Sec61 catalyzes the translocation of many secretory precursor proteins into the endoplasmic reticulum, as well as the insertion of transmembrane proteins into the cell and organellar membranes. Precursor proteins that possess weak signal peptides frequently require presence of the accessory membrane protein TRAP. Structural biology has recently established that TRAP shares several contact sites with Sec61, though not by an extended binding interface. However, how TRAP mechanistically supports the translocation of precursor proteins is still partially unresolved. Here, atomistic molecular dynamics simulations revealed that TRAP binding keeps Sec61 in a partially opened state, with looser packing of its transmembrane helices. TRAP maintained a partially opened Sec61 lateral gate and pore ring, shifting the plug helix towards an open conformation. These observations corroborate the existing model of how TRAP may support translocation of client precursor proteins with weak signal peptides.

1. Introduction

The universally conserved eukaryotic Sec61 translocon, or SecYEG in prokaryotes, mediates the translocation of secretory precursor proteins into either the lumen of the eukaryotic endoplasmic reticulum (ER) or into the prokaryotic periplasmic membrane, [1–4] serving to insert transmembrane proteins laterally into the ER membrane. More than 30% of eukaryotic proteins possess domains requiring ER protein import [5,6]. Sec-dependent protein translocation can occur in either a co- or post-translational manner, depending on the associated partner protein [4,7]. The co-translational mode is a ribosome-dependent process, where the signal peptides emerging at the ribosome exit tunnel are recognized by a cytosolic complex known as signal recognition particle (SRP) [8,9]. SRP then directs the ribosome-nascent chain complex (RNC) to the ER membrane by interacting with the SRP receptor, succeeded by RNC being transferred to the Sec61 channel positioned next to the ribosome exit tunnel, resulting in SRP being released and followed by signal peptide insertion into the channel [10,11]. In contrast, post-translational translocation takes place after translation is completed: it is an SRP-independent process wherein translocation of the completely synthesized polypeptide is supported by protein chaperones [7,11,12]. In eukaryotes, two further membrane proteins, Sec62 and Sec63, as well as the lumenal chaperone immunoglobulin heavy chain binding protein (BiP), are associated with Sec61 to activate the channel [12–14]. In fungi, two additional non-essential proteins, Sec71 and Sec72, are coordinated to Sec63 [4,12,15].

Sec61 is a hetrotrimeric complex that comprises of three subunits, in which [3,16] Sec61α in mammals, with homologues SecY in prokaryotes, or Sec61p in *S. cerevisiae*, is the central, essential subunit of this protein conducting channel. All of these homologues are composed of ten transmembrane helices (TMs), divided into two covalently linked N- (TM1-5) and C-terminal (TM6-10) halves surrounding a central pore [3, 17,18]. A so-called "pore-ring" is composed of six hydrophobic residues belonging to TMs 2, 5, 7, and 10 and is filled by a short helix "plug" halfway across the membrane [3,19]. The precursor polypeptides either translocate along the Sec61 pore or insert themselves sideways into the membrane via a "lateral gate" formed by helices TM2 and TM7; see Fig. 1(c) [17,18,20]. To facilitate protein transport, the plug must be displaced from the Sec61 pore, prompting Sec61 to transform into an open conformation[18,21,22]. In mammals, the central subunit, Sec61α, associates with Sec61β and Sec61γ subunits; the two linked halves of Sec61α are clamped together by Sec61γ, while the precise function of the β subunit remains unclear [3].

While the evolutionarily conserved Sec61 channel alone is generally sufficient to translocate signal peptides (SPs) of nascent presecretory polypeptides and TMs across or into the ER membrane, some polypeptide precursors with "weak" SPs cannot efficiently and independently translocate by Sec61, necessitating further assistance from additional factors, such as the heterotetrameric translocon-associated protein (TRAP), translocating chain-associated membrane protein (TRAM), and Sec62/Sec63 with BiP, which may interact with Sec61 to promote the translocation of these precursors. In vitro experiments have

* Corresponding author.
E-mail address: volkhard.helms@bioinformatik.uni-saarland.de (V. Helms).

https://doi.org/10.1016/j.bbamem.2025.184488
Received 15 July 2025; Received in revised form 5 November 2025; Accepted 23 November 2025
Available online 24 November 2025

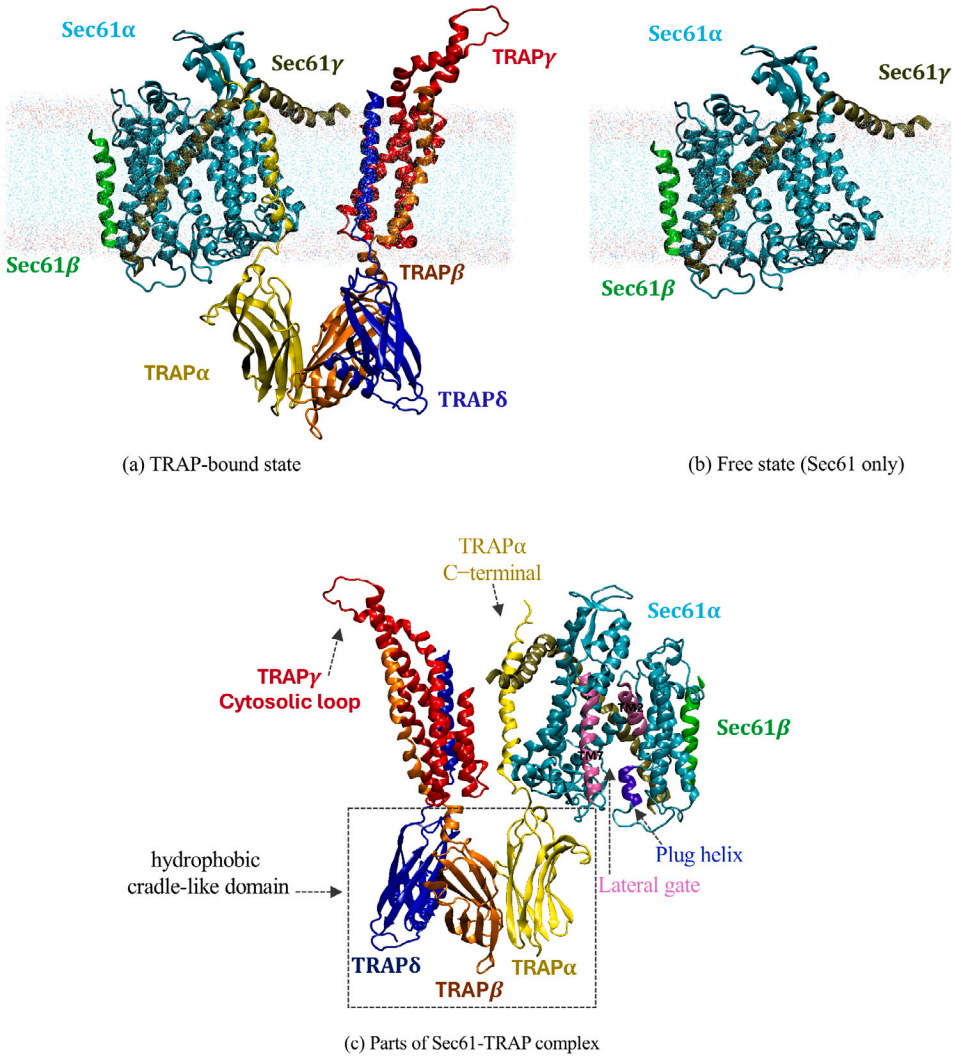

Fig. 1. Initial conformations of (a) TRAP-bound and (b) free states of Sec61. (c) The essential components of the Sec61-TRAP complex. Lipid molecules are shown as lines with their polar head groups in red. The various subunits are shown in different colors with "New Cartoon" representation using VMD, namely Sec61α (cyan), Sec61β(green), Sec61γ (tan), TRAPα (yellow), TRAPβ (orange), TRAPγ (red), and TRAPδ (blue). Water and ions are not shown for clarity.

suggested that the translocation of some weakly gating polypeptide precursors is aided by TRAP and BiP to facilitate Sec61 channel opening in a substrate-specific manner [19,23,24]. Here, classifying SPs as "weak" generally refers to the insufficient hydrophobic strength of the targeting signal, which proves essential for translocation via the channel, or for lateral membrane insertion. Proteomic data for human TRAP-dependent clients showed that weak signal peptides often possess weak α-helical propensity or hydrophobic strength, oftentimes due to a rather high glycine and/or proline content [24].

Structural biology has successfully revealed atomistic conformations of unbound and substrate-engaged Sec61, as well as its interactions with accessory membrane proteins [17,18,22,25,26]. Specifically, Karki et al. and Jaskolowski et al. provided structural insight into TRAP-assisted ribosome docking and nascent polypeptide insertion into Sec61 in a Sec61-OST-TRAP complex [27,28]. The oligosaccharyl-transferase (OST) complex located in proximity of Sec61 is observed in approximately 50% of translocon particles in mammalian cells and is responsible for the catalysis of co-translational N-glycosylation of substrates. The translocon-associated protein complex (TRAP) is an ER-resident auxiliary complex and consists of four membrane-anchored subunits: TRAPα, TRAPβ, TRAPγ and TRAPδ [29,30]. TRAPγ consists of a four helix TM bundle, while TRAP luminal domains α, β and δ form a hydrophobic cradle-like domain, as observed in Fig. 1(c), that is positioned at the exit of the Sec61 pore [28]. Jaskolowski et al. reported that the emerging nascent polypeptide interacts with the TRAP cradle-like domain, specifically with the TRAPα lumenal domain after plug displacement [28]. Additionally, Pauwels et al. reported that the TRAPα C-terminal domain and TRAPγ cytosolic loop interact with the ribosome. [31] Despite these current advances in structural research, how TRAP contributes mechanistically to protein translocation remains unclear [26–28,31,32].

Using multiple independent atomistic molecular dynamics (MD) simulations, Bhadra et al. studied the effect of accessory proteins Sec63 and Sec62 on the conformational dynamics of the yeast Sec61 translocon in the post-translational mode [33,34]. Specifically, conformational changes of the gating elements, namely lateral gate, pore ring region, and plug domain were monitored by measuring diagonal distances between pore -forming residues and their angular shifts along MD trajectories [33,34]. The simulations reproducibly demonstrated different mechanistic roles of Sec62 and Sec63 on the lateral gate conformation of Sec61, with results showing that Sec63's interaction with TM2 of Sec61 contributes to lateral gate opening. Moreover, it was revealed that a reorientation of TM4 of Sec61 resulted from interactions between TM3 of Sec63 and TM1 of Sec61 yielding an open pore conformation [33]. Computer simulation of the Sec62:Sec61 complex suggested that lateral gate opening towards the luminal side is aided by interactions of TM2 of Sec62 with TM7 of Sec61α [34].

Current research implementing a single-particle cryo-electron microscopy (cryo-EM) has yielded an atomic model of mammalian ribosome-bound Sec61-TRAP complex in which multiple interaction sites were identified between TRAP subunits, as well as with Sec61 and the ribosome [27]. Using atomistic and coarse-grained MD simulations, results revealed that TRAP induces a thinning of the surrounding lipid membrane, which could potentially affect the conformational dynamics of Sec61. To characterize the interactions between the Sec61-TRAP complex and ribosome, Karki et al. simulated the entire assembly of Sec61-TRAP and large ribosomal subunit for 100 ns while opting to keep the backbones of RNA and proteins restrained. The simulation suggested that the interactions of TRAP and Sec61 with the ribosome stabilize the complex and may be related to the translocation of TRAP-dependent polypeptides. To investigate the stability of the molecular interactions between Sec61, TRAP, and the ribosome, Karki et al. additionally performed unrestrained atomistic MD simulations of the complex and its subcomplexes embedded in a lipid bilayer, with these simulations revealing that TRAP stabilization strongly depended on ribosome anchoring of the TRAPα and TRAPγ subunits, in addition to interactions with Sec61. If ribosomal anchoring was not considered, the TM helix of TRAPα shifted towards other TMs of TRAP subunits. These MD simulations also showed that the binding of TRAP to the ribosome maintained and/or stabilized the initial open lateral gate conformation of Sec61: in particular, the TM2-TM7 distance, as compared to simulations of unbound Sec61 where the lateral gate usually closed. It was proposed that the lateral gate opening for specific SPs could be related to membrane thinning caused by a V-shaped characteristic conformation of TRAP, a cytosolic side interaction with both ribosome and Sec61. Notably, the initial structure determined by Karki et al. featured a closed plug and an open lateral gate conformation, such that TM2-TM7 COM distance: $\sim$ 2.4 nm. In contrast, the initial structure used in this current study had an open plug, while the lateral gate was not fully open and accommodated a signal peptide.

None of the aforementioned studies thoroughly focussed on how the conformational dynamics of Sec61 channel are affected by the TRAP complex; to this aim multiple atomistic molecular dynamics simulations were performed, starting from the cryo-EM structure of Sec61 bound to TRAP and of unbound Sec61, both embedded in a lipid bilayer, but in the absence of the ribosome. The simulations revealed how Sec61 gating elements, such as the pore, plug, and lateral gate, adapted their conformations due to either the presence or absence of the TRAP complex, respectively. Overall, it was observed that presence of TRAP stabilized open conformations of the lateral gate, pore ring, and plug helix, begetting a more loosely packed Sec61. All of this may plausibly aid in translocation of precursor peptides with weak SPs though this is beyond the scope of this study.

2. Materials and methods

2.1. Homology modeling

A cryo-electron tomography (cryo-ET) structure determined by Gemmer et al. of a human Sec61-TRAP translocon complex bound to a large multisubunit complex oligo-saccharyl transferase (OSTA) provided a near-complete atomic model (PDB ID: 8B6L) [26] with structural information on the assembly of the Sec61α, β and, γ subunits and TRAPα, β, γ and δ subunits, respectively. Here, our interest focused on the individual effect of the accessory protein TRAP on the Sec61 complex, necessitating the exclusion of the OSTA subunits present in 8B6L. The initial cryo-ET structure and the derived MD initial model used in the current study is pictured in Figure S1. The conformations of some missing parts of Sec61 were modeled using homology modeling with MODELLER 10.4 [35], incorporating another cryoEM structure of the Sec61 channel (PDB ID: 3JC2) [18]. Missing parts of the TRAP subunits were modeled as loop conformations, except for the unresolved long amino acid stretches at the N- and C-termini of the TRAP subunits that were omitted. This final conformation of Sec61, along with TRAP, was used as an input for subsequent MD simulations and termed as a "TRAP-bound" conformation. To observe putative structural relaxation of Sec61 in the absence of TRAP, the TRAP complex was deleted from this "TRAP-bound" state, which was labeled as the "free" state in our simulations.

2.2. Molecular dynamics (MD) simulations

The structural models of the Sec61-TRAP complex and of Sec61 alone were embedded in a POPC bilayer membrane using the CHARMM-GUI web portal [36]. The orientation of the protein structures in the lipid bilayer was determined by the PPM server [37]. The systems were hydrated and 150 mM of KCl solution was added to render the systems electrically neutral. The total number of atoms for the free and TRAP-bound states were 144,994 and 303,525, respectively; this includes 300 lipids and 31,912 water molecules in the free state, and 500 and 72,463 in the bound state, respectively. The two starting structures are illustrated in Fig. 1, with all essential parts of the Sec61-TRAP complex displayed in Fig. 1(c).

All MD simulations were carried out using GROMACS (version 2023.2) [38], with CHARMM36 force field for proteins [39] and lipids, [40] and TIP3P [41] model for water. The solvated systems were energy minimized using steepest descent for 5000 steps. Equilibration of 5 ns was done in six steps, with two NVT & four NPT steps, according to the standard CHARMM-GUI equilibration protocol, whereby harmonic restraints were applied to heavy atoms of the protein, planar restraints were put in place to hold the positions of head groups of the membrane bilayer along the z-axis, and fatty acid chain double bonds were maintained in cis configurations by dihedral restraints. The force constants of restraints on the protein backbone, side chains, and lipid molecules were slowly reduced from 4000 to 50 kJ/mol/nm^2, 2000 to 0 kJ/mol/nm^2, and 1000 to 0 kJ/mol/nm^2, respectively, as the equilibration progressed and the systems were relaxed. The Nosé-Hoover [42] thermostat, with a coupling constant of 1.0 ps at 303.15 K, and the Parrinello-Rahman [43] barostat at 1 bar were used to maintain temperature and pressure of the system. Finally, production runs were extended to 1 μs each in the NPT ensemble without any restraints. Short-range van der Waals interactions were calculated using a cutoff of 1.2 nm and long-range electrostatic interactions were treated with the particle-mesh Ewald (PME) method [44]. The LINCS algorithm was used to constrain bond lengths to their equilibrium values, with the time step set to 2 fs. Five independent MD simulations of 1000 ns length each were carried out for each system seeded with different initial random velocities.

Movie S1 shows an animation of Sec61-TRAP interactions in the MD1 simulation trajectory. Surprisingly, in three out of five MD simulations for the TRAP-bound case, the TRAP complex detached from Sec61 during the simulations and subsequently interacted with a periodic image of Sec61; see Figure S1 and Movie S2. This may possibly be an artifact of setting small box dimensions. These detachment simulations were ultimately not considered, and instead, three further independent MD simulations of the Sec61 were added, featuring a TRAP complex with a larger box size, with a total number of 418,525 atoms, including 700 lipid and 101,809 water molecules. In these simulations, no detachment of TRAP was observed. In total, the current study involved the generation and analysis of 10μs of trajectories in the production phases.

2.3. Simulation analysis

Simulation trajectories were analyzed using GROMACS (version 2023.2), as well as custom codes and scripts for analysis. Root mean square deviation (RMSD), radius of gyration (Rg), and root mean square fluctuations (RMSF) were calculated using the "gmx rms", "gmx gyrate", and "gmx rmsf" plugins of GROMACS. VMD software was used

for visualizing the structures. The local conformational dynamics of Sec61 was investigated using various distance and angle measurements such that helical axes were defined to connect the two end points of a transmembrane helix (TM), where the end point of a TM was defined as the center of mass of the Cα-atoms of its four terminal residues.

The radius (R) of the pore-ring region was obtained through a curve fitting approach, where the Cα atoms of the N-terminal pore-forming residues from transmembrane helices 2, 5, 7 and 10, respectively, and their contact residues within 0.5 nm distance were projected on the lipid bilayer plane, with the equation of a circle fitted to these projected points; see Figure S14a, with red spheres representing contact residues [33].

3. Results and discussion

At first, the global effect of TRAP on the conformational dynamics of Sec61 was characterized in terms of root mean square deviation (RMSD), radius of gyration (Rg), and root mean square fluctuations (RMSF).

RMSD and Rg reached plateau values after about 200 ns, as seen in Figs. 2 and S3, for both TRAP-bound and free states. The radius of gyration (Rg) for both systems, as seen in Figure S3, converged to similar Rg values of ~2.57 nm in all simulations, with and without TRAP. In addition, RMSDs of most individual TMs stabilized after about 200 ns, suggesting that the same conformational relaxation also applies to distance and angle measurements; see Figure S4. The only TM helices showing noticeable deviations or conformational dynamics after 200 ns were TM7 and TM10; see Figure S4. The density plots of local structural features obtained either from the time interval between 800–1000 ns or between 600–1000 ns are remarkably similar for both TRAP -bound and free states; see Figures S8 and S9. Thus, our simulations were considered to be well-converged on a 1 μs timescale and the last 400 ns were considered to characterize properties related to local flexibility.

3.1. Structural stability of the central channel-forming subunit (Sec61α) and interaction sites (ISs) between Sec61 and TRAP

The averaged RMSD from the initial structure that was based on the cryo-EM structure of a Sec61-TRAP-OSTA complex was lower for the simulations of the TRAP-bound state (~ 0.61±0.015 nm) than for the simulations of the free state (~ 0.73± 0.021 nm), indicating that presence of TRAP stabilized the Sec61 complex near its initial open conformation; see Figs. 2(a) and 2(b). RMSD alignments of the final conformations (t=1 μs) are shown in Figs. 2(c) and 2(d). The terminal ends of TM2, TM3, TM4, and TM7 deviated in both final conformations from the initial structure, but more strongly in the free state. While the plug helix mostly remained in place in both states, the two loops that connect the plug helix to the rest of Sec61α demonstrated more mobility in the free state than in the TRAP-bound state; see Figs. 2(c) and 2(d).

The cryo-ET structure (PDB ID 8B6L) [26] used as starting conformation reported three interaction sites between Sec61 and TRAP; see Fig. 3. (1) The C-terminal end of TRAPγ shares contacts with the N-terminus of Sec61γ in the membrane region. (2) The TRAPα subunit interacts with the second helix of the hinge region of Sec61α, while (3) its luminal domain interacts with the β-hairpin of the hinge region between TMs 5 and 6 of Sec61α. The cryo-EM structure of the ribosome-bound Sec61-TRAP complex obtained by Karki et al. [27] mentioned similar interaction sites of Sec61 with TRAP, reporting one additional interaction site between Sec61α and TRAPγ at the membrane interface (4).

To determine the stability of the contacts at the four interaction sites during the simulations, various center of mass distances between Sec61 and TRAP subunits were monitored by considering the Cα atoms of the interacting residues at TM helix termini, as well as all interacting atoms in loop residues, or in other regions. At interaction site 1 (IS1), contact distances were measured between the Cα atoms of the N-terminal residues of Sec61γ:Met1-Val4 and the C-terminal residues of TRAPγ:Leu180-Gly183. At IS2, the interacting residues were nTM8 of Sec61α:Asp357-Hsd360 and the C-terminus of the long TM helix F (cTMF) of TRAPγ:Phe154-Leu157. At IS3a, contact distances were evaluated between the second helix of the hinge region (2hH), namely Sec61α:Lys226-Tyr235 and the N-terminus of the TM helix of TRAPα:Gly205-Ile208. Also, the distance was scanned between the center of mass of the second hinge helix (2hH) Sec61α:Lys226-Tyr235 and the nTM of TRAPα+connecting loop, TRAPα:195Thr-Ile208. This distance is referred to as IS3b; see Fig. 3.

The TRAPα luminal domain contains two short loops 1 and 2 between β-sheets 1 and 2, as well as sheets 3 and 4, and a longer third loop between β-sheets 5 and 6. To obtain detailed information about this interaction site 4 (IS4), the interactions of the β-hairpin at the hinge region of Sec61α were probed with these three TRAPα luminal loops, with these interaction sites termed as IS4a, IS4b, and IS4c; see Fig. 3.

As shown in Fig. 4, the contact distance at IS1 was not stable around its initial value of 1.12 nm and fluctuated considerably throughout independent simulations. Figures S5 and S6 display all interaction sites, with the interacting residues highlighted in magenta. In simulations 2, displayed with the red curve, and 4, displayed with the blue curve, the distance initially increased, then started to decrease at around 950 ns to its initial; see Fig. 4(a). In contrast, at IS2, as detailed in Fig. 4(b), the distances remained closer to the initial value, though sometimes were enlarged by 0.5–1 nm, and proved more stable, except for during MD3, as displayed with the green curve, where the distance increased from 1.44 to approximately 4.5 nm.

At IS3a, almost all initial contacts were maintained, as seen in Fig. 4(c), except in MD4, illustrated with the blue curve, where the distance increased near the end of the simulation. Interestingly, in MD4, the distance at IS1 began to decrease simultaneously, possibly suggesting a compensating effect; see Fig. 4(a). In all simulations, the contact distances at IS3b demonstrated a similar tendency as IS3a, but at somewhat greater values; see Figs. 4(d) and S5d. Notably, this loosening of contact during MD4 was similar to that at IS3a.

In MD3, the distance between the N-terminal residues of Sec61γ and the C-terminal end of TRAPγ at IS1, as well as the distance between nTM8 of Sec61α and the C-terminal of cTMF of TRAPγ at IS2, increased roughly at the same time, as visualized by the green TRAP-b3 curve. Yet, in MD3, the contacts at IS3a and IS3b were stable between the nTM region of TRAPα and the second helix of the hinge region of Sec61α. Conversely, IS1 and IS2 were stable during MD4 whereas IS3a and IS3b contacts ruptured.

In combination, this suggests that if contacts between Sec61 and TRAP subunits loosen at one interaction site, either at the cytosolic face of the membrane, at the transmembrane interface, or at the lumen, they may remain stable at other interaction sites. Thus, overall, TRAP was demonstrated to stably interact with the Sec61α hinge region, which is known to bridge the pseudo-symmetrical N- and C-terminal halves of Sec61.

The aforementioned distances at IS1, IS2, IS3a, and IS3b are all located in the transmembrane regions of the Sec61 and TRAP subunits. To ascertain the stability of the interactions of Sec61α with the luminal domain of TRAPα, the distances between the β-hairpin of the hinge region of Sec61α and the three loops, loops 1–3 in Fig. 3, were also monitored within the six β-sheets of the TRAPα luminal domain, as shown in Figs. 4(e), S6a, and S6b, with the interacting residues highlighted in magenta in Figures S5e, S6e, and S6f. During almost all independent simulations, the distances fluctuated similarly at IS4a, IS4b, and IS4c from their initial values, as marked by the black curve in Figs. 4, S5 and S6. Figs. 4(e) and S6a show that the contact distances IS4c, with loop 3, and IS4a, with loop 1, fluctuated less from their initial value than at IS4b, with loop 2, potentially due to its orientation towards the translocon side; see Fig. 3, at IS4. On average, at IS4, the distances stabilized at around 3.0 nm.

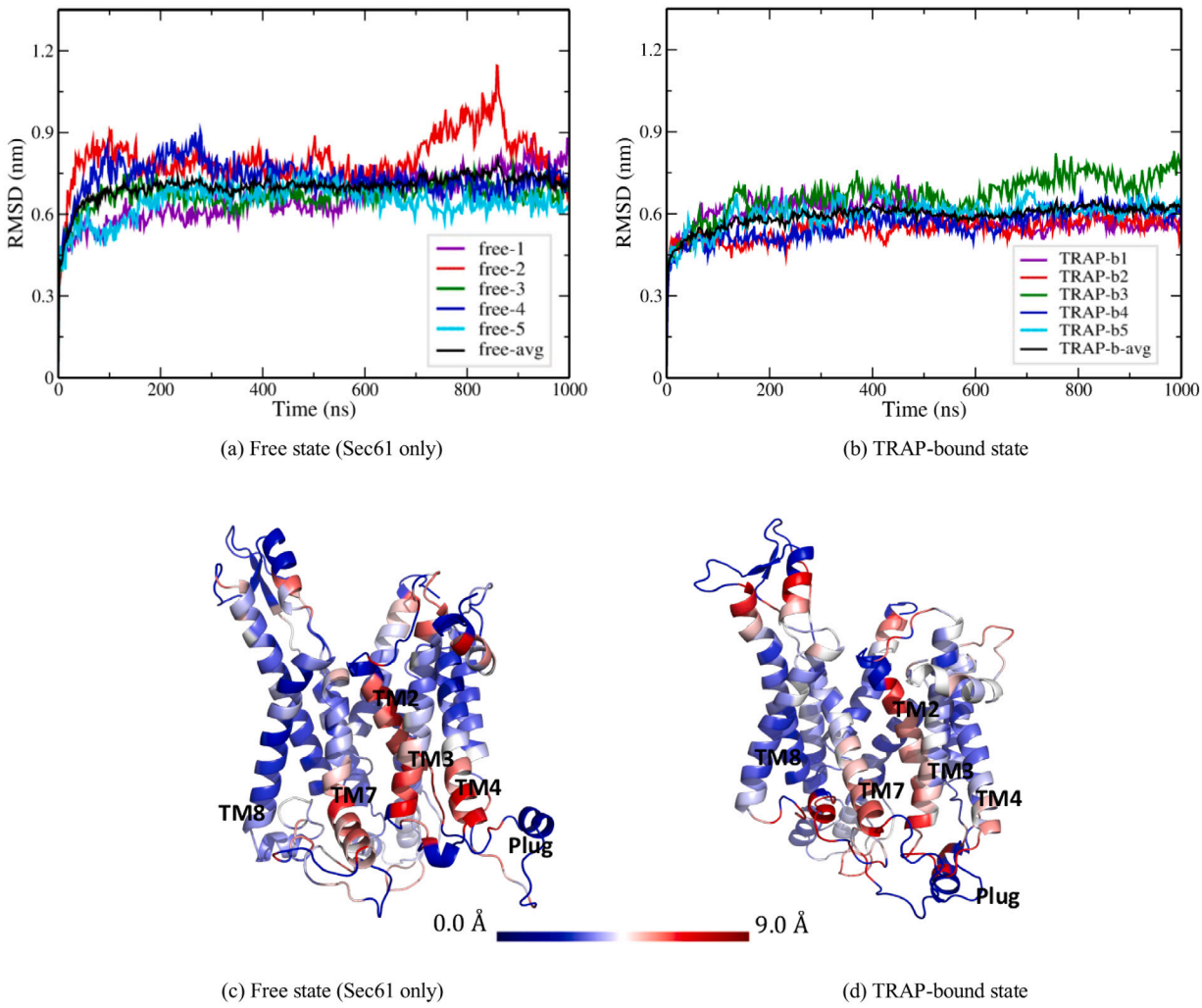

Fig. 2. Time evolution of the root mean square deviation (RMSD) of Sec61α with respect to the starting structure. Results are shown for trajectories 1 to 5, respectively, for (a) "free" Sec61 without TRAP and (b) "TRAP-b" (TRAP-bound) states. Structural deviations in final conformations (t=1 μs) of Sec61α in (c) free and (d) TRAP-bound state with respect to the starting structure are colored according to RMSD values of their Cα atoms.

Interestingly, during the simulations, the ER-lumenal loop 7, namely the loop between TM helices 7 and 8, of Sec61α moved closer to the TRAP luminal domain, the TRAP cradle. Thus, the distances between luminal loops 1–3 of TRAPα and the ER-lumenal loop 7 between β-sheets of TM7 and TM8 were monitored, this distance being termed as IS5; see Fig. 3. Independently of the scale, the curves showed similar trends for all simulations, as observed in Figs. 4(f), S6c and S6d, and resembled IS4. The interacting residues are highlighted in magenta color in Figures S5f, S6g and S6h. Figs. 4(f), S6c and S6d clearly illustrate that the distances at IS5c, with respect to loops 7 and 8 of Sec61α to luminal loops of TRAPα, decreased below the initial values, which suggests a putative interaction between Sec61 and TRAP at this site. These contacts proved to be mostly hydrophobic. To analyze a specific contact in greater detail, looking at Figure S7, the hydrogen bonds at interaction site 5 (IS5c) were plotted and these interacting residues in the final conformation of MD simulation were located.

Although previous studies presenting cryo-EM structures of Sec61:TRAP complexes did not mention the specific IS5c interaction site, it is speculated that loop 7 could play an important role in TRAP-dependent, mediated translocation of weak signal peptides. Previously, Tretter et al. also reported the importance of loop 7 in facilitating protein import, as a Sec61 mutant model lacking this loop resulted in a strong deficit in post-translational translocation [45]. Overall, it can be concluded that the conformation of Sec61α is not only affected by TRAP via the hinge region of Sec61α, at the loop between TM5/6, but also by the loop between TM7/8. According to Jaskolowski et al. [28], mutations in the highly conserved loop 3 between β-sheets 5 and 6 of the TRAPα luminal domain exacerbated the ER stress phenotype and induced developmental defects in *C. elegans*. This suggests that TRAP binds jointly to the translating ribosome with its cytosolic part and to the translocating pore with its luminal part, supporting its role in protein biogenesis [46].

3.2. Structural stability of Sec61 in absence and presence of TRAP

Fig. 5 illustrates the conformational flexibility of each residue of Sec61α by their root mean square fluctuations (RMSF) in individual trajectories, with the structural alignment being conducted using Sec61 only. In free and TRAP-bound states, as seen in Fig. 5(a) and Fig. 5(b), respectively, the fluctuations were of almost similar magnitude, except for the regions at interaction sites 2 and 5 (IS2 and IS5) and the plug region. Residues in these regions proved more flexible in the free state, pictured by the pink curve, than in the TRAP-bound state, observed by the green curve; see zoom view of interaction sites 2 and 5 in Fig. 5(c).

3.3. Conformational changes of the gating elements of the Sec61α

In order for protein translocation to occur, structural rearrangements in the critical gating elements of Sec61 must take place, namely

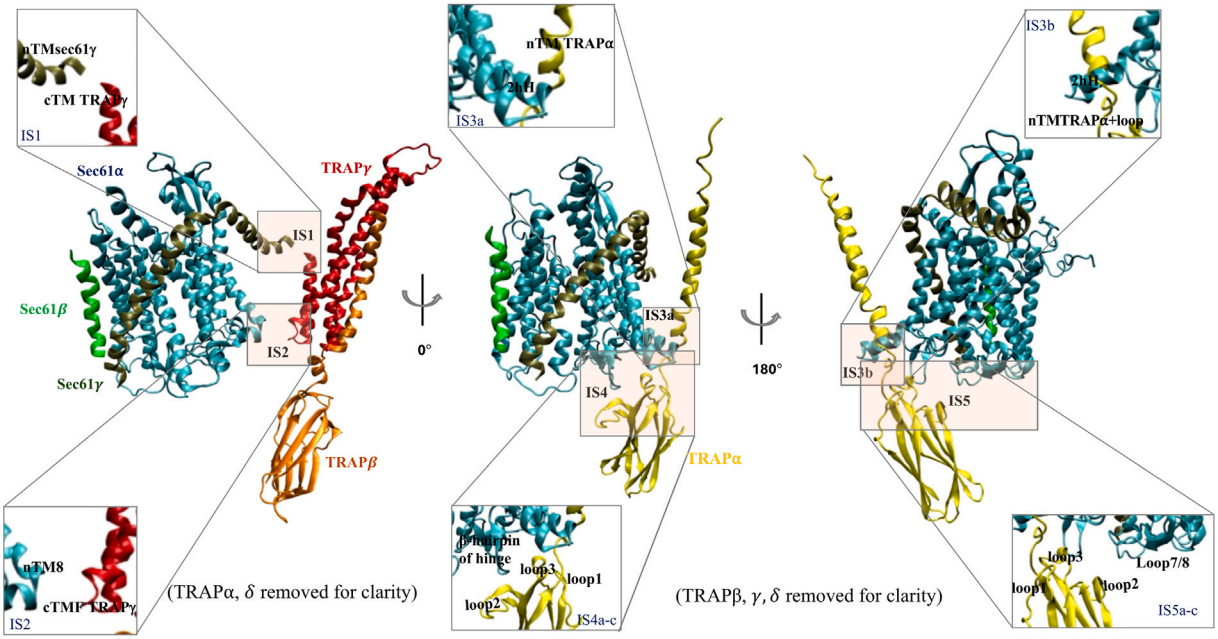

Fig. 3. Overview of interaction sites of TRAP and Sec61 complex and magnified views. Individual subunits are colored and labeled differently in "new cartoon" representation.

in the lateral gate, pore ring, and in the plug domain, halfway across the membrane.

As previously mentioned, polypeptides may either translocate along the Sec61 pore into the ER lumen or laterally insert themselves into the membrane [3,4,19,47] via the lateral gate that is formed by TMs 2 and 7 of Sec61α. According to previous findings, the signal peptide recognition and insertion site is located at the interface of the lateral gate helices towards the cytosolic ends of the translocon [22,48]. To capture the conformational dynamics of the lateral gate, the distance $d_{cTM2\text{-}nTM7}$ was determined between the center of mass of the four Cα atoms, equal to one helical turn, at the C-terminus of TM2 (Gln92-Ala95) and those at the N-terminal end of TM7 (Phe284-Ser287). The time evolution of $d_{cTM2\text{-}nTM7}$ is shown in Figs. 6(a) and 6(b) for both states. Figure S10a highlighted the residues selected to measure the distance between the lateral gate helices. Averaged over five independent simulations, the distance decreased by similar degree for TRAP bound (~0.24 nm) and unbound (~0.29 nm) states, as compared to the starting structure (1.77 nm) shown in Figure S5a. Similar to $d_{cTM2\text{-}nTM7}$, the center of mass distance between the cytosol-facing N-terminal helical turns of TM2 and TM8, $d_{cTM2\text{-}cTM8}$ shown in Figure S10, reduced by similar amounts from the initial value, 2.00 nm, pictured by the black dot, to 1.76 ± 0.17 nm and 1.73 ± 0.18 nm in both bound and free states, respectively. Furthermore, to investigate the conformational dynamics of the lateral gate, the distance was measured between the C-terminal helical turns of helices TMs 3 and 7 $d_{cTM3\text{-}cTM7}$ at the luminal side; see Figure S11. This distance decreased by ~ 0.94 nm and ~ 0.68 nm for TRAP-bound and unbound systems, as seen in Figure S11, from the initial value, 2.12 nm. The time evolution plots pictured in Figure S11b and S11c show that two free simulations, MD3 and MD5, fluctuated around the initial value, resulting in increased distances; in Figure S11b, the black solid curve shows the average over five simulations relative to the TRAP-bound case.

It has been revealed experimentally that there exists characteristic spontaneous opening and subsequent closure of the SecYEG pore: a rare, slow process occurring on a seconds time scale [49]. In our case, the free state simulation was commenced from a pre-expanded conformation and followed its conformational transitions towards a more closed state. As observed in our previous studies of Sec61:Sec63 and Sec61:Sec62 complexes from yeast [33,34], this relaxation occurs quite rapidly on a microsecond time scale, though not within 1 microsecond. Notably, a similar relaxation towards the closed state of the lateral gate was reported by Allen et al. for bacterial SecYEG, which can be observed in Figure 2C of the study [50].

With respect to the starting structure, the aforementioned decrease of lateral gate distances between the terminal ends of the lateral gate helices could also be coupled to an orientational shift of either one or both of the lateral gate TMs. As shown in Figures S9 and S12, this was validated by computing the two angles between the TM2 or TM7 helical axes and the vector normal to the lipid bilayer: θ_{TM2} and θ_{TM7}. In the initial structure, these two tilt angles determined as θ_{TM2}= 45.3°and θ_{TM7}= 29.7°. ; yet, the probability distribution plots in Figure S9a and S12b show that θ_{TM7} did not show any significant deviation, expanding only by ~ 2°for both bound and unbound states and stabilized close to its initial value. In contrast, θ_{TM2} decreased on average in both free and bound states; see Figure S9a. In the bound state, on average, θ_{TM2} increased by approximately 4° relative to the free state; see Figure S9a, in which the θ_{TM2} values obtained in three out of five TRAP-bound simulations were close to the value in the initial structure, as marked by the black dot. Therefore, TM2, a part of the lateral gate, displayed a larger orientational shift with respect to the normal vector of the lipid bilayer in the free state than in the TRAP-bound state: these structural deviations in lateral gate helices are illustrated in Figs. 2(c) and 2(d).

As discussed, the pore-ring of the human Sec61 translocon consists of six hydrophobic residues at the N-termini of TMs 2, 5, 7, and 10, namely Ile81(TM2), Val85(TM2), Ile179(TM5), Ile183(TM5), Ile292(TM7), and Leu449(TM10); these six residues are marked by the red spheres in Fig. 7(a). Prospective conformational changes of the pore-ring residues in TRAP-bound or unbound states were characterized by measuring the two diagonal distances $d_{nTM5\text{-}nTM7}$ and $d_{nTM2\text{-}nTM10}$ between the center of mass of the Cα atoms in the N-terminal helical turns of TM5 (Ser177-Ser180) and TM7 (Phe284-Ser287), as well as between TM2 (Ile81-Ile84) and TM10 (Gly442-Thr445), respectively, as shown in Fig. 7(a). The probability distribution plot for the free state in Fig. 7(b) illustrates that $d_{nTM5\text{-}nTM7}$ decreased by ~ 0.18 nm on average from the initial value, 1.76 nm, to 1.58 ± 0.15 nm, while presence of TRAP stabilized $d_{nTM5\text{-}nTM7}$ at 1.74 ± 0.18 nm. On the other hand, $d_{nTM2\text{-}nTM10}$ decreased from the initial value, 1.91 nm, to 1.67 ± 0.15 nm in the free state and to

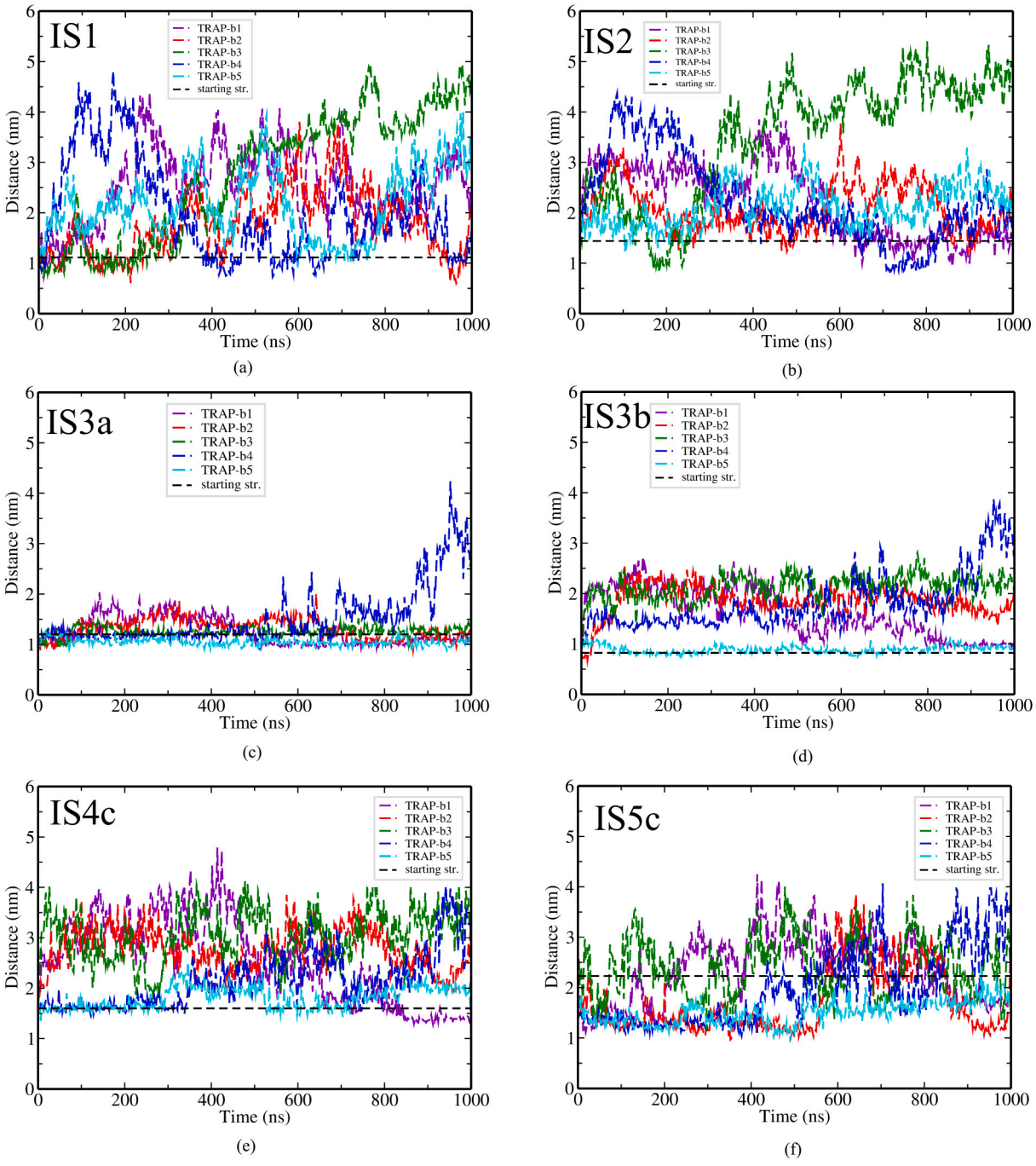

Fig. 4. Time evolution of contact distances shown in Fig. 3. (a) Interaction site 1 (IS1-Sec61γ:Met1- Val4 to TRAPγ:Leu180-Gly183, (b) interaction site 2 (IS2-Sec61α:Asp357-Hsd360 to TRAPγ:Phe154-Leu157, (c) interaction site 3a (IS3a-Sec61α:Lys226-Tyr235 to TRAPα:Gly205- Ile208), (d) interaction site 3b (IS3b-Sec61α:Lys226-Tyr235 to TRAPα:195Thr-Ile208) (e) interaction site 4 (IS4c-Sec61α:Thr200-Phe209 to TRAPα:Ile159-Pro168) (f) interaction site 5 (IS5c-Sec61α:Trp324-Pro337 to TRAPα:Ile159-Pro168). The dashed black horizontal lines denote the respective values in the starting structure.

1.57 ± 0.10 nm in the TRAP-bound case; see Fig. 7(d). On average, this observed decrease was greater in the bound case after t=650 ns; see Figures S13c and S13d. In a published *in silico* study of Sec61:Sec62 complexes, Bhadra et al. observed a similar behavior of the accessory protein Sec62 on Sec61, whereby the diagonal distance $d_{nTM2\text{-}nTM10}$ decreased by approximately 0.3 nm and 0.2 nm in both the presence or absence of Sec62, respectively, while $d_{nTM5\text{-}nTM10}$ increased in the presence of Sec62. This suggests that TRAP affects pore conformation in a similar manner to Sec62. Additionally, the distance $d_{nTM5\text{-}nTM10}$, see Fig. 7(c), and the radius (R) of the pore-ring region, see Figure S14, were computed; interestingly, $d_{nTM5\text{-}nTM10}$ also expanded in two (MD3; green and MD5; cyan) out of five TRAP-bound simulations, resulting in a total increase in $d_{nTM5\text{-}nTM10}$ in the TRAP-bound state, with an average of 1.75 ± 0.07 nm, as seen in Fig. 7(c), compared to the free state, with an average of 1.67 ± 0.01 nm. Also, in the time dependent plots, the distance $d_{nTM5\text{-}nTM10}$ fluctuated less and demonstrated higher stability for almost all replicas as compared to $d_{nTM5\text{-}nTM7}$ and $d_{nTM2\text{-}nTM10}$; see Figures S13e and S13f.

Averaged over five simulations, the pore ring radii for free and bound states were 0.848 ± 0.037 and 0.868 ± 0.034 nm, respectively, with the pore diameter proving roughly the same in both free and TRAP-bound states. The direct interaction of the TRAPα subunit with

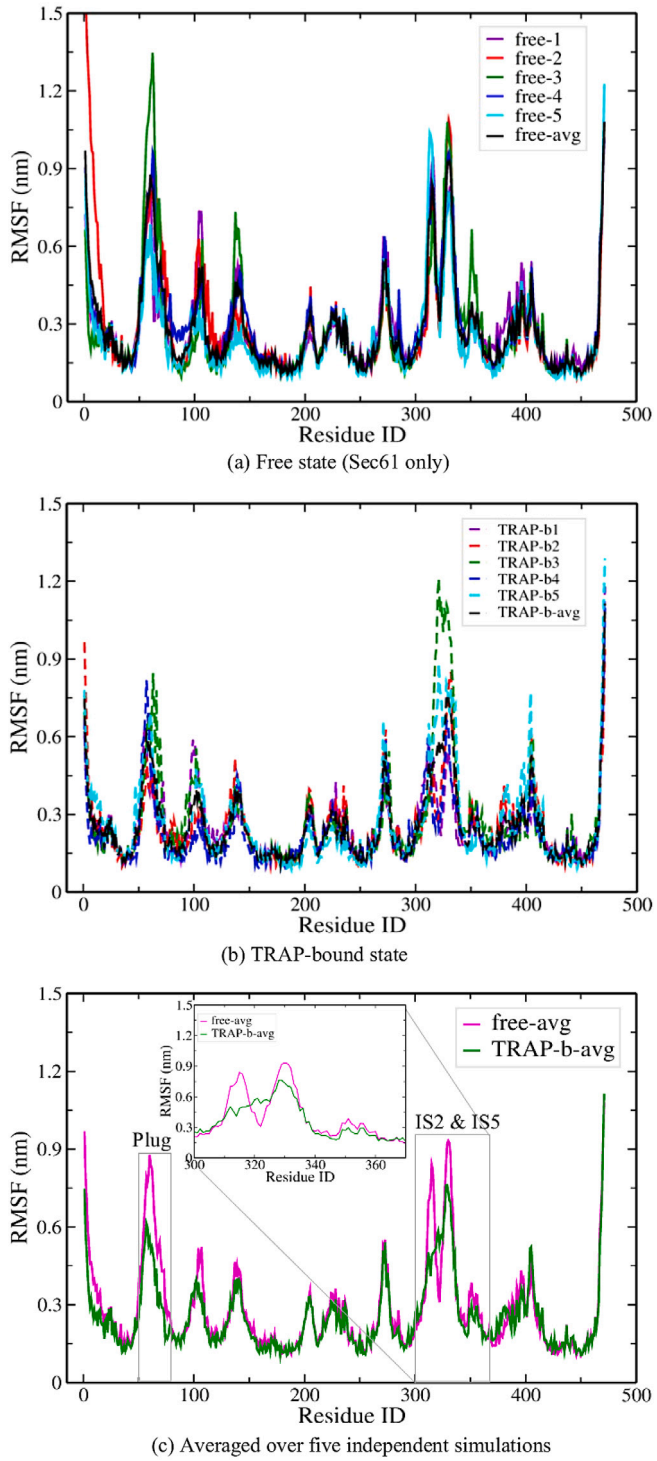

Fig. 5. Residue specific root mean squared fluctuation (RMSF) profile of Sec61α residues during simulations in (a) free state (without TRAP) and in (b) TRAP-bound state. (c) Averages over the five simulations of each system with a zoom view of interaction sites 2 and 5, as well as a highlighted plug region. The plug, IS2, and IS5 residues are more flexible in the free state (pink curve) than in the TRAP-bound state (green curve).

the TM5 hinge region of Sec61α may explain the stability of these pore-ring distances, as seen in Fig. 7, in the TRAP-bound case, which characterizes its role in maintaining the channel pore in an open conformation. In a simulation study of the Sec61:Sec63 complex, Bhadra et al. observed a shrinking of the pore-ring radius by about 0.2 nm in both states, on average. In an *E. coli* model, Berg et al. reported that the opening formed by the ring ranges from 0.5 to 0.8 nm in diameter.[3] Lang and co-workers estimated that the opening diameter of the dynamic Sec61 channel varies from 0.5 to 0.7 nm and 1.2 to 1.4 nm for the main and subconductance states [11], respectively.

3.4. Structural rearrangements of TMs in Sec61/pore and plug in TRAP bound and unbound states

It has been established that the ten transmembrane helices (TMs) of the central subunit Sec61α consist of two covalently linked N- and C- terminal halves: TMs 1–5 and TMs 6–10, as seen in Figure S15a [3,17,18,26]. At the opposite side of the lateral gate, these two halves are connected by an external loop formed between TM5 and TM6, termed the hinge region of Sec61α. Interestingly, this part forms direct contacts with the TRAP subunit as the two halves are clamped together by the Sec61γ subunit [26]. As reported, polypeptides either translocate along the Sec61 pore into the ER or laterally insert into the membrane via a lateral gate: both mechanisms involve relative motions of these pseudo-symmetric halves; see Figure S15a [3,19]. Superimposing the final conformations for TRAP-bound and free states of Sec61α at t=1 μs, larger conformational changes were revealed in the N-terminal half, where the TMs of the N-terminal half of Sec61α shifted more in the unbound case than in the TRAP bound state; see Figure S15j. This observation substantiates the findings of previous studies, in which the N-terminal half was reported to be more mobile, while the C-terminal half remained rather static [3,19]. These results indicate that conformational changes of the pseudo-symmetric halves of Sec61α around the lateral gate perform an essential role in channel opening and closing, as well as maintaining structural stability.

To uncover the local dynamics of these two halves of Sec61α around the lateral gate helices TM2 and TM7 in the simulations, the center of mass distances of TM2 to the N-terminal half TMs 1–5 were monitored, as well as those of TM7 to the C-terminal half TMs 6–10 of Sec61α; all atoms of TMs were considered, as shown in Figure S15. Table 1 lists the average over five simulations, along with standard deviations of these distances during the last 400 ns of the simulations and their initial values. The probability distribution plots displayed in Figure S15, together with Table 1, reveal that most distances shrank noticeably in the free case, as shown in Figures S15b-i with the black solid curve, relative to the initial values shown in Figures S15b-i with the black dashed curve. In contrast, in the presence of TRAP, most center of mass distances remained stable and a few distances involving the lateral gate helices, namely $d_{TM2\text{-}TM4}$, $d_{TM7\text{-}TM8}$, and $d_{TM7\text{-}TM9}$, even expanded relative to the initial values. This suggests that TRAP is mediating a loosening in the Sec61 channel architecture, echoing previous findings [19,23,24]. Taking into account previous reports on the client spectrum of TRAP [23,24], it can be speculated that such a loosely packed channel can indeed support the translocation of weak SPs.

To verify if the simulations reach a state similar to any available Sec61 structure in the total absence of TRAP, the idle-state ribosome-Sec61 complex (3J7Q) was compared with our simulations, using the center of mass distance between lateral gate helices and by describing the position of the plug helix. The TM2-TM7 distance in the cryo-EM structure 3J7Q was observed to be 1.10 nm. The lateral gate distance in our "free" state simulations was found to be similar to the idle-state ribosome-Sec61 complex (3J7Q), such that MD1=1.09 nm, MD2=1.21 nm, and MD3=1.03 nm; see Figure S16 which shows a structural superposition of Sec61 alpha in some of our simulations with cryo-EM structure 3J7Q. In our starting model, this distance was 1.46 nm. However, the plug was observed as distant from the Sec61 pore, similarly to the starting structure, in all of our simulations, as opposed to the idle-state ribosome-Sec61 complex (3J7Q). Overall, the simulations showed that relative motions between the lateral gate

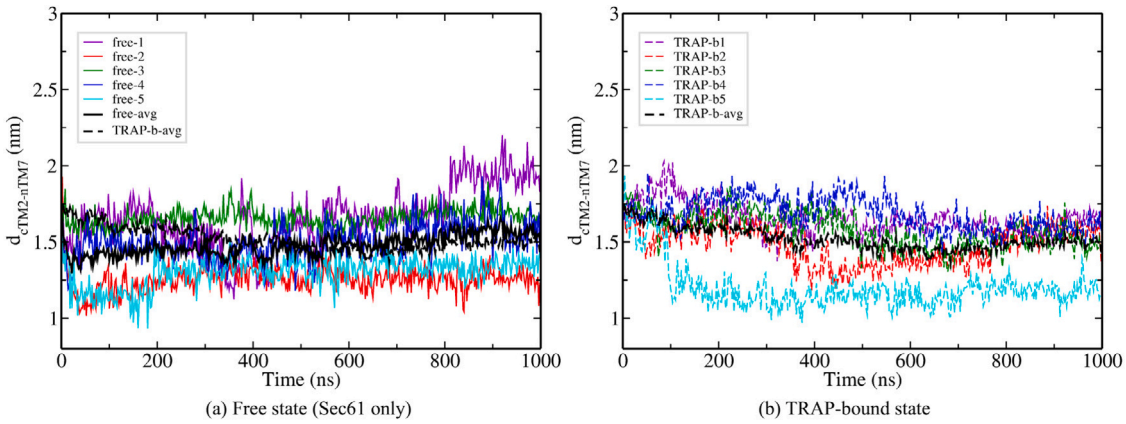

Fig. 6. Variation of the center of mass distance between the ends of lateral gate helices TM2 and TM7 $d_{cTM2\text{-}nTM7}$ during five independent MD simulations for (a) "free" (solid lines) and (b) TRAP-bound (dashed lines) states.

helices, with respect to each other and other TMs, govern the dynamics of the Sec61 pore.

In the cryo-EM structure of the idle or inactive state of Sec61, the helical plug is located just below the pore-ring and moves away from the pore in the SP-engaged state [17,22]. To capture potential structural changes of the plug helix within our study, the center of mass distance between residues of the pore-ring and of the plug was calculated; see Fig. 8(a). The distance increased in both TRAP-bound and unbound states relative to the initial value; see Figs. 8(c) and 8(d) to observe the time evolution of this distance. Initially, it was speculated that in the absence of TRAP, the plug may move closer to the pore in the Sec61 closed plug condition. Instead, on average over five simulations, the plug showed a displacement 0.2 nm farther from the Sec61 pore in the free state than in the TRAP-bound case; see Fig. 8(b). To explain this mechanistically, the final structures of the free and TRAP-bound states were inspected, represented by the red solid and dashed curves, respectively, in Fig. 8(b) for MD2. In the free state, the plug moved outwards from the Sec61 channel and migrated between the Sec61β and Sec61γ subunits, changing its orientation parallel to the lipid bilayer; see Figures S17a and S17b. These conformational changes of the plug were associated with an increase in the center of mass distance between Sec61β and the C-terminal half of Sec61γ ($d_{Sec61\beta-Sec61\gamma}$) by approximately 0.5 nm on average when compared to the starting structure, as seen in Figs. 9(a) and 9(b), revealing a high overall flexibility of these subunits in the free state, as seen in Figures S18a and S18b. The probability distribution plot displayed in Fig. 9(a) yields average values with standard deviation for free and bound states of 2.79 ± 0.27 and 2.57 ± 0.23 nm, respectively, over five simulations. In turn, an increased flexibility of Sec61β and γ may explain the increased distance between Sec61β and Sec61γ in the free state; see Fig. 9(a). This supports the results illustrated in Figs. 5(c), S18c, and S18d, in which the plug helix was shown to fluctuate more strongly in the unbound state. However, the plug moved closer to the C-terminus of Sec61γ in the TRAP-bound case, as observed in Fig. 9(b), and created more H-bonds, as seen in Figure S19. Similarly to $d_{plug-cTMSec61\gamma}$, stabilization of the plug in an open form in the TRAP-bound case is also seen in Fig. 9(c), which displays the probability distribution of center of mass distance between the plug and the β-hairpin of hinge region, with the time dependence of these distances shown in Figure S20. In the bound state, the distance was shorter, at ~0.20 nm, than in the initial structure, represented by the black dot in Fig. 9(c) , while in the free state, the distance expanded by ~0.75 nm on average from the starting structure. The average values with standard deviation in the free and TRAP-bound states were 2.60 ± 0.87 and 1.66 ± 0.34 nm, respectively. This suggests that in the bound state, in the Sec61 open plug condition, the plug is stabilized in the open form; see Figures S17c and S17d.

Ultimately, the simulations suggest that the plug, as well as the Sec61β and Sec61γ subunits, are considerably more mobile in the free state. Hence, the stability and flexibility of the Sec61β and Sec61γ subunits may directly impact plug dynamics. In cryo-EM structure 8B6L, OST subunits are present near the Sec61β and Sec61γ subunits, the plug helix, and the TRAP luminal domain, which were missing in our starting conformation. In 8B6L, the plug also forms contacts with the luminal OSTC- β-hairpin. Omitting the OST complex in our simulations could be one reason for the increased flexibility of these regions, which were also observed in interaction sites involving the luminal portion of TRAPα. It should be noted that $d_{pore\text{-}plug}$, as shown in Figs. 8(b) and 8(c), shows a similar trend to some curves, such as MD2 displayed in red in Figure S20a and MD3 in blue in Figure S20c; this is observed both for the full simulation (0 to 1μs), as well for their converged parts; see Figs. 9(b) and 9(c). This suggests that the plug conformational dynamics in these simulations correspond to the conformational flexibility of these three regions, i.e. of the pore, C-terminus of Sec61γ, and beta-hairpin of the hinge. In the simulations, the pore-to-plug distance expanded in the unbound state, but the plug did not orient towards the β-hairpin of the hinge the C-terminus of Sec61γ, which have been associated with an open plug conformation. [3,26] In the bound case, it approached the C-terminus of Sec61γ, the β-hairpin of the hinge, or the TRAPα luminal loops, as illustrated in Figure S21, where the distance from the plug to the TRAPα luminal loops follows a trend similar to that of the β-hairpin of the hinge and loop7/8 in Figs. 4(e) and 4(f).

Thus, it can be inferred that the plug conformation is influenced by presence of the nearby TRAP subunit. In the TRAP-bound state, the plug was found to be stabilized in the open position, with Sec61γ and Sec61β also observed to be stabilized in TRAP-bound simulations. Monitoring the interaction site distances (between the β-hairpin and 2nd helix of the hinge, the end terminal distance between Sec61γ and TRAPγ, and loop7/8) and the distance to the plug helix showed that TRAP impacted the conformation of the Sec61 channel, either through its transmembrane domain or through the luminal domain.

3.5. Limitations

In the cryo-ET structure of the Sec61-TRAP-OSTA translocon complex, the cytosolic domain of TRAPγ was found to make contacts to the rRNA expansion segments ES20L and ES26L, to ribosomal protein L38, and to the oligosaccharyltransferase complex (OSTA), which is located near the Sec61 plug helix region; ES20L and ES26L are multinucleotide insertions located in eukaryotic rRNAs, where L signifies the large subunit. Pauwels et al. [31] and Jaskolowski et al. [28] also emphasized the importance of the TRAPα and γ subunits for positioning the TRAP complex in proximity to Sec61 via interactions with the ribosome in

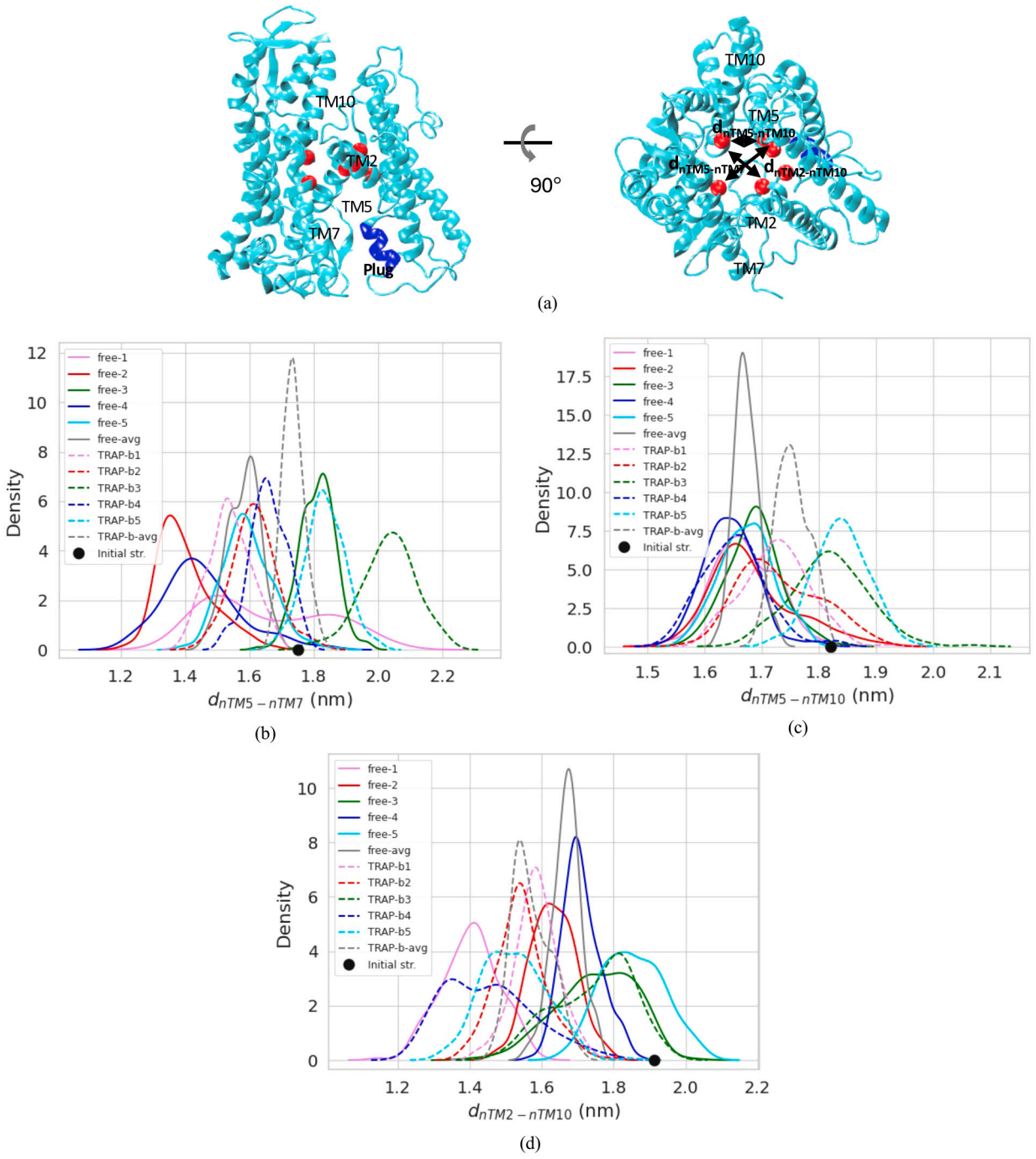

Fig. 7. (a) Representation and definition of the pore to plug distances. (b) The probability distributions of pore to plug distances ($d_{Pore\text{-}Plug}$) calculated over five independent MD simulations and their averages, for "free" state (solid lines) and "TRAP-bound" (dashed lines) state. Black dot represents the distance value in the starting structure. Time dependence of $d_{Pore\text{-}Plug}$ profile for (c) "free" state (solid lines) and (d) "TRAP-bound" (dashed lines) state, respectively.

the cytosolic region. Additionally, the cytosolic loops of Sec61α, loop 6/7 and 8/9, have been reported to be involved in ribosome binding. In our case, the absence of ribosome and OSTA subunits are suspected to have resulted in enlarged fluctuations at some interaction sites.

The lateral gate distances $d_{cTM2\text{-}nTM7}$ and $d_{cTM2\text{-}cTM8}$ reduced by similar amounts from the initial value in both bound and free states; this reduction may be explained by the absence of signal peptide inside the channel and of other accessory subunits in the simulation system.

In particular, cardiolipin was shown to be essential for the stability of the Sec61 channel, as well as for optimal translocation or insertion in the membrane [51]. However, cardiolipin possesses complex physicochemical properties and diffuses more slowly in lipid bilayers than simpler phospholipids, which complicates conformational sampling in molecular dynamics simulations [52]. Instead, this study implemented 1-palmitoyl-2-oleoyl-sn-glycero-3-phosphocholine (POPC), a phosphaditylcholine, as a homogenous lipid model commonly used in MD simulation studies.

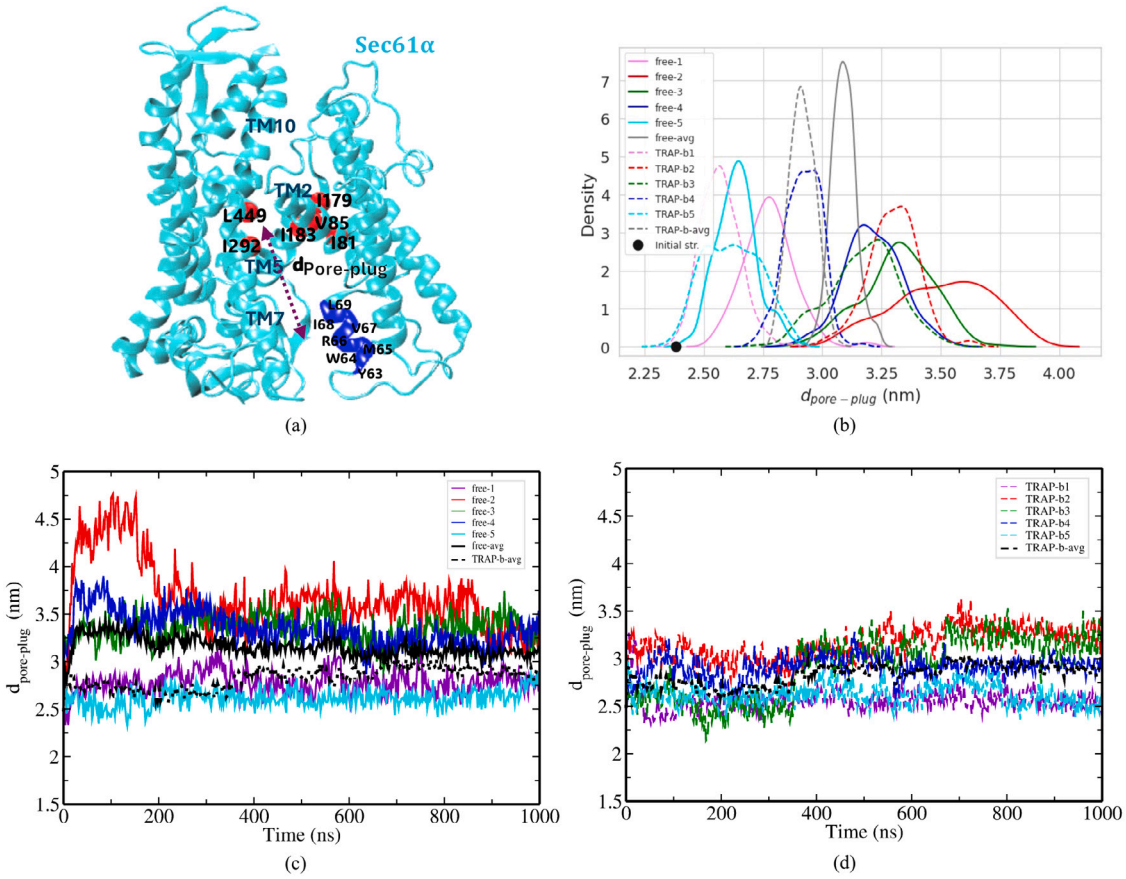

Fig. 8. (a) Representation and definition of the distances $d_{nTM5\text{-}nTM7}$, $d_{nTM5\text{-}nTM10}$, and $d_{nTM2\text{-}nTM10}$ of the channel pore. As shown, these distances were defined between the center of mass of Cα atoms of N-terminal helical turns of pore forming residues from transmembrane helices 2, 5, 7, and 10, respectively. The plug helix is shown in blue color. (b-d) Probability distributions of these distances across the channel pore during last 400 ns of five independent MD simulations for "free" (solid lines) and "TRAP-bound" (dashed lines) states. The black dot represents the distance value in the starting structure.

4. Conclusions

Within this study, a cryo-EM structure of the Sec61$\alpha\beta\gamma$: TRAP complex was used as the initial starting conformation. Ribosomes and OSTA also present in the cryo-EM map were omitted to simplify the system. The simulations revealed considerably similar interactions between Sec61 and TRAP as detected in the cryo-EM studies. Some contacts at the interaction sites remained tightly bound, while other contacts became looser; this may be an artifact of omitting other subunits present in the cryo-EM map.

MD simulations of a Sec61$\alpha\beta\gamma$:TRAP complex suggested that TRAP stabilizes an open conformation of the central Sec61α pore and of the plug via delicate molecular interactions that involve its TM region, as well as its soluble protein domains. However, the free state started from the TRAP-bound state and a structural relaxation towards the closed state is expected. Overall, inter-helical TM distances were enlarged in the TRAP-bound complex, suggesting that binding of TRAP induces a loosening of the Sec61α conformation. Omitting ribosome and OSTA domains in the simulations enabled us to carry out simulations of a more manageable subsystem, yet this strategy also resulted in larger fluctuations at certain contact sites identified in the experiments. It remains unclear as to how TRAP assistance is connected to intrinsic conformational physico-chemical features of its client precursor proteins.

CRediT authorship contribution statement

Nidhi Sorout: Writing – original draft, Visualization, Validation, Methodology, Investigation, Formal analysis, Data curation, Conceptualization. **Volkhard Helms:** Writing – review & editing, Supervision, Resources, Project administration, Investigation, Funding acquisition, Conceptualization.

Declaration of competing interest

The authors declare that they have no known competing financial interests or personal relationships that could have appeared to influence the work reported in this paper.

Acknowledgments

This work was supported by Deutsche Forschungsgemeinschaft, Germany through He3875/15-1. The authors thank Prof. Friedrich Förster for early access to their structural data on the Sec61:TRAP assembly and Anna Elizabeth Schmitz for comments on the text.

Appendix A. Supplementary data

Supplementary material related to this article can be found online at https://doi.org/10.1016/j.bbamem.2025.184488.

Data availability

Data will be made available on request.

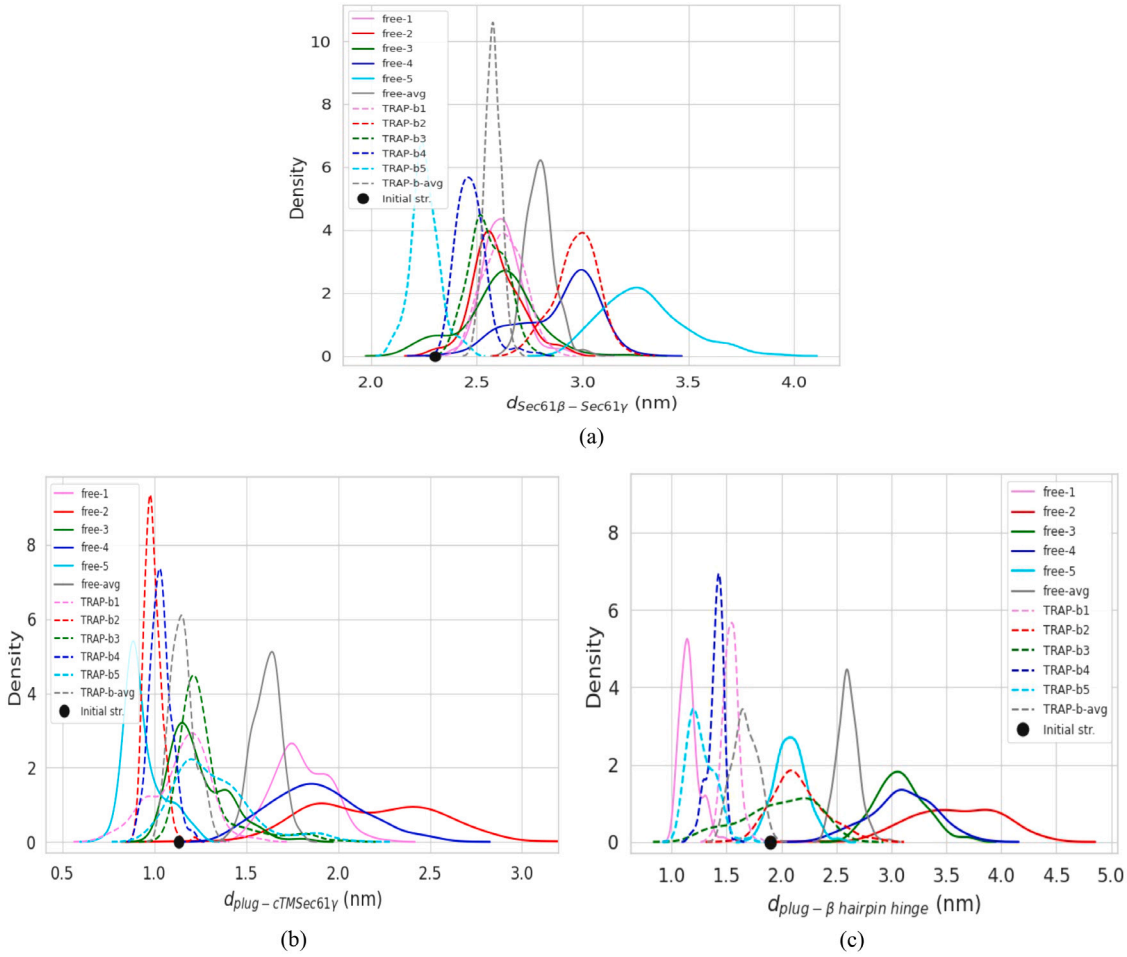

Fig. 9. Probability distributions of the center of mass distance between (a) Sec61β and C-terminal half of Sec61γ i.e. $d_{Sec61\beta-Sec61\gamma}$, (b) plug to C-terminus of Sec61γ $d_{plug-cTMSec61\gamma}$, and (c) plug to β-hairpin of the Sec61α hinge region $d_{plug-cTMSec61\gamma}$ during last 400 ns of five independent MD simulations for "free" (Sec61 without TRAP: solid lines) and "TRAP-b" (TRAP-bound: dashed lines) states. Black dots represent the distance values in the starting structure.

References

[1] E. Park, T.A. Rapoport, Mechanisms of Sec61/SecY-mediated protein translocation across membranes, Annu. Rev. Biophys. 41 (2012) 21–40.

[2] S. Itskanov, E. Park, Mechanism of protein translocation by the Sec61 translocon complex, Cold Spring Harb Perspect Biol. (2022) a041250.

[3] B. Van den Berg, W.M. Clemons, I. Collinson, Y. Modis, E. Hartmann, S.C. Harrison, T.A. Rapoport, X-ray structure of a protein-conducting channel, Nature 427 (2004) 36–44.

[4] A.R. Osborne, T.A. Rapoport, B. van den Berg, Protein translocation by the Sec61/SecY channel, Annu. Rev. Cell. Dev. Biol. 21 (2005) 529–550.

[5] S. Lang, R. Zimmermann, Mechanisms of ER protein import, Int. J. Mol. Sci. 23 (2022) 5315.

[6] S. Tan, H.T. Tan, M.C. Chung, Membrane proteins and membrane proteomics, Proteomics 8 (2008) 3924–3932.

[7] J. Dudek, S. Pfeffer, P.H. Lee, M. Jung, A. Cavalie, V. Helms, F. Forster, R. Zimmermann, Protein transport into the human endoplasmic reticulum, J. Mol. Biol. 427 (2015) 1159–1175.

[8] P. Walter, G. Blobel, Translocation of proteins across the endoplasmic reticulum. II. Signal recognition protein, SRP, mediates the selective binding to microsomal membranes of in-vitro-assembled polysomes synthesizing secretory protein, J. Cell. Biol. 91 (1981) 551–556.

[9] M. Halic, R. Beckmann, The signal recognition particle and its interactions during protein targeting, Curr. Opin. Struct. Biol. 15 (2005) 116–125.

[10] G. Kramer, A. Shiber, B. Bukau, Mechanisms of cotranslational maturation of newly synthesized proteins, Annu. Rev. Biochem. 88 (2019) 337–364.

[11] S. Lang, S. Pfeffer, P.H. Lee, A. Cavalié, V. Helms, F. Förster, R. Zimmermann, An update on Sec61 channel functions, mechanisms, and related diseases, Front. Physiol. 8 (2017) 887.

[12] X. Wu, C. Cabanos, T.A. Rapoport, Structure of the post-translational protein translocation machinery of the ER membrane, Nature 566 (2019) 136–139.

[13] H.A. Meyer, et al., Mammalian Sec61 is associated with Sec62 and Sec63, J. Biol. Chem. 275 (2000) 14550–14557.

[14] J. Tyedmers, M. Lerner, C. Bies, J. Dudek, M.H. Skowronek, I.G. Haas, et al., Homologs of the yeast sec complex subunits Sec62p and Sec63p are abundant proteins in dog pancreas microsomes, Proc. Natl. Acad. Sci. USA 97 (2000) 7214–7219.

[15] R.J. Deshaies, S.L. Sanders, D.A. Feldheim, R. Schekman, Assembly of yeast sec proteins involved in translocation into the endoplasmic reticulum into a membrane-bound multisubunit complex, Nature 349 (1991) 806–808.

[16] M. Gemmer, F. Förster, A clearer picture of the ER translocon complex, J. Cell Sci. 133 (2020) jcs231340.

[17] R.M. Voorhees, I.S. Fernańdez, S.H.W. Scheres, R.S. Hegde, Structure of the mammalian ribosome-Sec61 complex to 3.4 åresolution, Cell. 157 (2014) 1632–1643.

[18] R.M. Voorhees, R.S. Hegde, Structure of the Sec61 channel opened by a signal peptide, Sci. 351 (2016) 88–91.

[19] N. Sorout, V. Helms, Toward understanding the mechanism of client-selective small molecule inhibitors of the Sec61 translocon, J. Mol. Recognit. 38 (2025) e3108.

[20] C. Ma, X. Wu, D. Sun, E. Park, M.A. Catipovic, T.A. Rapoport, N. Gao, L. Li, Structure of the substrate-engaged SecA-SecY protein translocation machine, Nat. Commun. 10 (2019) 2872.

[21] P.F. Egea, R.M. Stroud, Lateral opening of a translocon upon entry of protein suggests the mechanism of insertion into membranes, Proc. Natl. Acad. Sci. USA 107 (2010) 17182–17187.

[22] M. Gogala, T. Becker, B. Beatrix, J.-P. Armache, C. Barrio-Garcia, O. Berninghausen, et al., Structures of the Sec61 complex engaged in nascent peptide translocation or membrane insertion, Nat. 506 (2014) 107–110.

[23] R.D. Fons, B.A. Bogert, R.S. Hegde, Substrate-specific function of the translocon-associated protein complex during translocation across the ER membrane, J. Cell. Biol. 160 (2003) 529–539.

[24] D. Nguyen, R. Stutz, S. Schorr, S. Lang, S. Pfeffer, H.H. Freeze, F. Foïster, V. Helms, J. Dudek, R. Zimmermann, Proteomics reveals signal peptide features determining the client specificity in human TRAP-dependent ER protein import, Nat Commun. 9 (2018) 3765.
[25] S. Pfeffer, L. Burbaum, P. Unverdorben, M. Pech, Y. Chen, R. Zimmermann, R. Beckmann, F. Förster, Structure of the native Sec61 protein-conducting channel, Nat. Commun. 6 (2015) 8403.
[26] M. Gemmer, M.L. Chaillet, J. van Loenhout, R. Cuevas Arenas, D. Vismpas, M. Gröllers-Mulderij, F.A. Koh, P. Albanese, R.A. Scheltema, S.C. Howes, A. Kotecha, et al., Visualization of translation and protein biogenesis at the ER membrane, Nature 614 (2023) 160–167.
[27] S. Karki, M. Javanainen, S. Rehan, D. Tranter, J. Kellosalo, J.T. Huiskonen, L. Happonen, V. Paavilainen, Molecular view of ER membrane remodeling by the Sec61/TRAP translocon, EMBO Rep. 24 (2023) e57910.
[28] M. Jaskolowski, A. Jomaa, M. Gamerdinger, S. Shrestha, M. Leibundgut, E. Deuerling, N. Ban, Molecular basis of the TRAP complex function in ER protein biogenesis, Nat. Struct. Mol. Biology 30 (2023) 770–777.
[29] S. Pfeffer, J. Dudek, M. Schaffer, B.G. Ng, S. Albert, J.M. Plitzko, W. Baumeister, R. Zimmermann, H.H. Freeze, B.D. Engel, F. Förster, Dissecting the molecular organization of the translocon-associated protein complex, Nat. Commun. 8 (2017) 14516.
[30] E. Hartmann, D. Görlich, S. Kostka, A. Otto, R. Kraft, S. Knespel, E. Bürger, T.A. Rapoport, S. Prehn, A tetrameric complex of membrane proteins in the endoplasmic reticulum, Eur. J. Biochem. 214 (1993) 375–381.
[31] E. Pauwels, N.R. Shewakramani, B. De Wijngaert, A. Camps, B. Provinciael, J. Stroobants, K.U. Kalies, E. Hartmann, P. Maes, K. Vermeire, K. Das, Structural insights into TRAP association with ribosome-Sec61 complex and translocon inhibition by a CADA derivative, Sci. Adv. 9 (2023) eadf0797.
[32] A. Russo, Understanding the mammalian TRAP complex function (s), Open Biol. 10 (2020) 190244.
[33] P. Bhadra, L. Yadhanapudi, K. Römisch, V. Helms, How does Sec63 affect the conformation of Sec61 in yeast? PLoS Comput. Biol. 17 (2021) e1008855.
[34] P. Bhadra, K. Römisch, V. Helms, Effect of Sec62 on the conformation of the Sec61 channel in yeast, Biochim. Biophys. Acta, Biomembr. 1864 (2022) 184050.
[35] B. Webb, A. Sali, Comparative protein structure modeling using MODELLER, Curr. Protoc. Protein. Sci. 86 (2016) 2.9.1–2.9.37.
[36] S. Jo, T. Kim, W. Im, Automated builder and database of protein/membrane complexes for molecular dynamics simulations, PloS One 2 (2007) e880, pmid:17849009.
[37] M.A. Lomize, I.D. Pogozheva, H. Joo, H.I. Mosberg, A.L. Lomize, OPM database and PPM web server: resources for positioning of proteins in membranes, Nucleic Acids Res. 40 (D1) (2012) D370–D376.
[38] M.J. Abraham, T. Murtola, R. Schulz, S. Páll, J.C. Smith, B. Hess, E. Lindahl, GROMACS: High performance molecular simulations through multi-level parallelism from laptops to supercomputers, SoftwareX (2015) 1–2, 19–25, http://dx.doi.org/10.1016/j.softx.2015.06.001.
[39] R.B. Best, X. Zhu, J. Shim, P.E. Lopes, J. Mittal, M. Feig, et al., Optimization of the additive CHARMM all-atom protein force field targeting improved sampling of the backbone ϕ, ψ and side-chain $\chi 1$ and $\chi 2$ dihedral angles, J. Chem. Theory Comput. 8 (2012) 3257–3273, pmid:23341755.
[40] J.B. Klauda, R.M. Venable, J.A. Freites, J.W. O'Connor, D.J. Tobias, C. Mondragon-Ramirez, et al., Update of the CHARMM all-atom additive force field for lipids: validation on six lipid types, J. Phys. Chem. B 114 (2010) 7830–7843, pmid:20496934.
[41] W.L. Jorgensen, J. Chandrasekhar, J.D. Madura, R.W. Impey, M.L. Klein, Comparison of simple potential functions for simulating liquid water, J. Chem. Phys. 79 (1983) 926–935.
[42] D.J. Evans, B.L. Holian, The nose-hoover thermostat, J. Chem. Phys. 83 (1985) 4069–4074.
[43] M. Parrinello, A. Rahman, Polymorphic transitions in single crystals: A new molecular dynamics method, J. Appl. Phys. 52 (1981) 7182–7190.
[44] T. Darden, D. York, L. Pedersen, Particle mesh Ewald: An N · log (N) method for Ewald sums in large systems, J. Chem. Phys. 98 (1993) 10089–10092.
[45] T. Tretter, F.P. Pereira, O. Ulucan, V. Helms, S. Allan, K.U. Kalies, K. Romisch, ERAD and protein import defects in a sec61 mutant lacking ER-lumenal loop 7, BMC Cell Biol. 14 (2013) 1–14.
[46] X. Li, O.A. Itani, L. Haataja, K.J. Dumas, J. Yang, J. Cha, S. Flibotte, H.J. Shih, C.E. Delaney, J. Xu, L. Qi, Requirement for translocon-associated protein (TRAP) α in insulin biogenesis, Sci. Adv. 5 (2019) eaax0292.
[47] A.K. Corsi, R. Schekman, Mechanism of polypeptide translocation into the endoplasmic reticulum, J. Biol. Chem. 271 (1996) 30299–30302.
[48] K. Plath, W. Mothes, B.M. Wilkinson, C.J. Stirling, T.A. Rapoport, Signal sequence recognition in posttranslational protein transport across the yeast ER membrane, Cell. 94 (1998) 795–807.
[49] E. Mercier, X. Wang, M. Maiti, W. Wintermeyer, M.V. Rodnina, Lateral gate dynamics of the bacterial translocon during cotranslational membrane protein insertion, Proc. Natl. Acad. Sci. 118 (2021) e2100474118.
[50] W.J. Allen, R.A. Corey, P. Oatley, R.B. Sessions, S.A. Baldwin, S.E. Radford, R. Tuma, I. Collinson, Two-way communication between SecY and SecA suggests a Brownian ratchet mechanism for protein translocation, Elife 5 (2016) e15598.
[51] S. Ryabichko, V.D.M. Ferreira, H. Vitrac, R. Kiyamova, W. Dowhan, M. Bogdanov, Cardiolipin is required in vivo for the stability of bacterial translocon and optimal membrane protein translocation and insertion, Sci. Rep. 10 (2020) 6296.
[52] R.N. Lewis, R.N. McElhaney, The physicochemical properties of cardiolipin bilayers and cardiolipin-containing lipid membranes, Biochim. et Biophys. Acta (BBA)-Biomembranes 1788 (2009) 2069–2079.